

# **FURTHER UNDESTANDING OF Ti-6Al-4V SELECTIVE LASER MELTING USING TEXTURE ANALYSIS**

M.Simonelli\*, Y.Y. Tse\*, C. Tuck†

\*Department of Materials, Loughborough University, LE11 3TU, UK

†Additive Manufacturing and 3D Printing Research Group, Faculty of Engineering, The University of Nottingham, Nottingham, NG7 2RD, UK

REVIEWED, Accepted August 22, 2012

## **Abstract**

Selective laser melting (SLM) has shown to be an attractive manufacturing route to produce Ti-6Al-4V components. In the present study, the relation between the texture evolution and a particular set of process parameters adopted for the production of near fully dense components was investigated. The aim of this investigation was to understand which microstructural features can be tailored during the SLM production. The microstructural characterisation of the as-built components was carried out using various microscopy techniques including optical, scanning electron and transmission electron microscopy. Phases and texture analysis were carried out using backscattered electron imaging and electron backscattered diffraction. It was found that the components consist of  $\alpha'$  martensitic phase precipitated from prior  $\beta$  columnar grains. It was found that the  $\alpha'$  martensitic laths develop from the parent  $\beta$  grains following the Burgers orientation relationship. The texture of the prior  $\beta$  phase was calculated and compared to the measured  $\alpha'$  texture. It was found that at each layer processing the  $\alpha'$  texture is retained and variant selection takes place. The observed microstructural details will be discussed in relation to the SLM parameters.

## **1. Introduction**

Selective laser melting (SLM) is a layer by layer additive manufacturing technique based on an infra-red fibre laser that creates solid layers from loose powder material and joins them in an additive manner. In principle, a thin layer of loose powder is initially levelled across a process platform and once the powder bed is ready selected areas of it are melted and consolidated line by line by a scanning laser. As soon as this layer is formed, new loose powder is deposited and melted on top of the layer below. Repeating this basic principle for multiple additive layers any 3D component can then be created, saving waste material and energy consumption when compared to traditional processing techniques [1]. As the energy delivered by the laser is fully controllable SLM has shown the possibility to fabricate near fully dense objects made of a broad range of metals generating interest within the aerospace and medical devices areas of application [2,3]. However, the complexity of the processing/microstructure and properties relationships makes SLM a manufacturing technology that has to yet be fully understood. For example, the microstructure of SLM Ti-

6Al-4V is not homogeneous due to the line- and layer-wise building strategy. The planes perpendicular to the building platform of as fabricated components always show large elongated prior  $\beta$  grain boundaries that are filled with acicular  $\alpha'$  martensitic laths as a consequence of the thermal history experienced by the layers [3-5]. The origin of this microstructure can be explained as follow: as the laser hits the powder bed the grains in the previous layers transform to the  $\beta$  phase field. Heat is then gradually conducted away vertically through the build and the grains can solidify and grow epitaxially along the build direction in the  $\beta$  phase field [3,4]. As the laser moves following a pre-set scanning pattern the  $\beta$  grain growth freezes and  $\alpha'$  martensitic phase originates within the  $\beta$  grains due to the imposed cooling rate. This fine microstructure is responsible for the reported low ductility of the as-built components whereas the vertical prior  $\beta$  columnar grain boundaries have been indicated as preferential regions for crack propagation and possible source of mechanical anisotropy [3,6]. Interestingly, it has been reported that despite the fact that each layer is thermally affected by the deposition of subsequent one or more layers, the morphology and size of the  $\alpha'$  grains remains the same throughout the whole sample showing no dependence on the sample size [4,7]. The planes parallel to the building platform reveal the laser scan tracks and the  $\alpha'$  grains within prior  $\beta$  grain boundaries delineating the top of the prior columnar  $\beta$  grains. Even if the aim of SLM is to produce fully dense solid objects, typically lenticular pores oriented horizontally between two processed layers (inter-layer porosity) or rounder voids characterise all the as fabricated builds [4,7]. Numerous studies have focused on tuning several process parameters in order to develop a suitable processing window to reduce porosity: laser scan speed, hatch spacing and scan strategy have shown to play an important role in the densification mechanism of SLM parts [8-10].

A systematic understanding of their contribution to the microstructure of SLM Ti-6Al-4V is however still required. This study focuses on the crystallographic texture evolution of Ti-6Al-4V produced by selective laser melting and attempts to clarify whether and which microstructural features could be possibly tailored during the building process.

The aim of the present study is to understand:

- Texture evolution of the as fabricated components in relation to the adopted process parameters
- Variant selection mechanism at the basis of the  $\beta/\alpha'$  transformation that occurs at each layer processing

## **2. Materials and Methods**

### **2.1 Powder Material**

The starting material was a pre-alloyed plasma atomized Ti-6Al-4V grade 23. The powder was supplied by LPW, UK. In order to choose a suitable layer thickness, the powder size and distribution were initially determined using a Malvern MasterSizer 2000. The measured particle size distribution was within 15 and 70  $\mu\text{m}$ , but, approximately 75% of the

examined particle size ranged between 25 to 50  $\mu\text{m}$ . Particles appear spherical, smooth with few smaller condensed particles attached to bigger particles (Figure 1). The microstructure of the starting powders consisted of lamellar  $\alpha$  phase with only a limited amount of retained  $\beta$  phase present (less than 4%). This may be due to the high cooling rate experienced by the powder during plasma atomization. The powder material microstructure is shown in Figure 2.

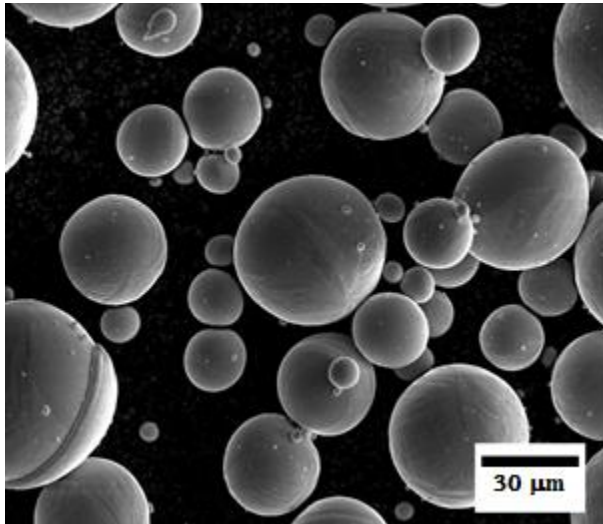


**Figure 1:** Shape and morphology of the starting powder bed

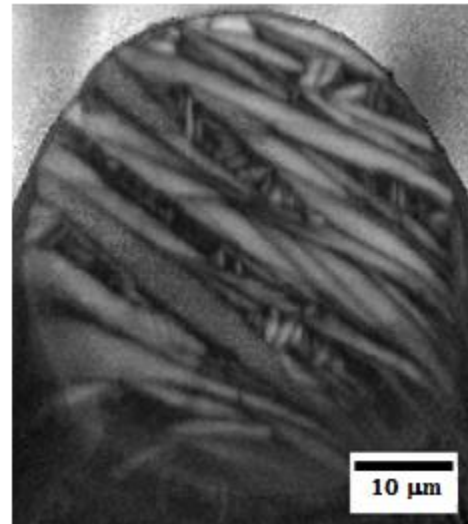


**Figure 2:**  $\alpha$ -image quality of an ion-beam milled Ti-6Al-4V plasma atomised particle

**Table 1:** Renishaw SLM250 Process Parameters

Laser Power, P (W)	200
Hatch Spacing, h ( $\mu\text{m}$ )	100
Point Distance, ( $\mu\text{m}$ )	50
Exposure Time, ( $\mu\text{s}$ )	220
Layer Thickness, ( $\mu\text{m}$ )	50
Scan Strategy	meander
Building Plate Temperature, ( $^{\circ}\text{C}$ )	65

## **2.2 Selective Laser Melting**

Simple cubic components of  $1\text{ cm}^3$  were built using a Renishaw SLM250. The machine is equipped with a fibre modulated pulse laser, with a maximum power of 200 W. The wavelength of the laser is 1070 nm. A series of experiments were performed to establish a processing window that could minimize residual porosity and that lead to the choice of the processing parameters summarized in Table 1. A multi-directional meander scan strategy was used, i.e. the laser scan direction was rotated by  $67^{\circ}$  at each layer in order to reduce the content of residual stresses. The cubes were built directly on top of a Ti- 6Al-4V build plate pre-heated at  $65^{\circ}\text{C}$  inside protective atmosphere back filled with Ar gas.

### **2.3 Optical and Electron Microscopy**

The microstructure of the as-built components was studied on specimens taken from the frontal section, i.e. planes parallel to the building direction. All sample surfaces were prepared by standard metallographic preparation procedures and then etched in Kroll's solution for optical/SEM. The microstructure of the components was examined in a Reichert-Jung MEF3 optical microscope and a Carl Zeiss (Leo) 1530 VP FEG-SEM system, which had a field emission source. Energy dispersive X-ray Spectroscopy (EDX) was used to identify the chemical composition of the powder, built components and the existence of the secondary phases. The distribution of crystallographic orientations of the sample crystals, i.e. the texture, was studied using electron back-scatter diffraction (EBSD) analysis available on the FEI Nova 600 Nanolab Dualbeam FIB/FEG-SEM system with EDAX EBSD camera. Data were processed using the TSL acquisition and data analysis software and MATLAB (The Mathworks, Inc., Natick, MA). In order to be able to fit the mounted samples onto the 70° pre-tilted (optimise EBSD data collection) aluminium holder, the mount was ground sideways. The scanning step size for EBSD was of 0.3µm. In order to gain a further understanding of the fine microstructure, thin TEM disks were prepared. Electropolishing was carried out in a temperature range of -20 to -30°C at 20V with the A2 electrolyte supplied by Struers. The TEM analyses were performed on a JEOL 2000FX TEM operated at 200 kV.

### **2.4 Automatic reconstruction of prior $\beta$ grain orientations**

Since the joining of adjacent layers occurs in the  $\beta$  phase field at elevated temperature, it is of interest to reconstruct the crystallographic texture of the prior  $\beta$  columnar grains. In this study, the reconstruction of the  $\beta$  grains was based on the Burgers crystallographic relationship that governs the  $\beta \rightarrow \alpha$  phase transformation for which the  $(0001)_\alpha // (110)_\beta$  and  $\langle 11\bar{2}0 \rangle_\alpha // \langle 111 \rangle_\beta$ . It is reported in fact that when residual  $\beta$  phase is not present (as expected for as-built SLM components) the nucleation of  $\beta$  grains from the  $\alpha$  laths follows the Burgers orientation relationship [11,12]. Orientations of the parent  $\beta$  grains were computed considering every triplet of neighboring  $\alpha'$  variants in the EBSD dataset. The  $\alpha'$  orientation was initially expressed by a rotation matrix using the three Euler angles between the principal crystallographic axes for each  $\alpha'$  grain and certain axes fixed by the geometry of the specimen. Using the Burgers orientation relationship six possible parent phase ( $\beta$  grain) orientations were generated for every  $\alpha'$  belonging to the triplet. Only the solution common to the triplet (or the solution with the least misorientation) was taken as orientation of the parent  $\beta$  phase from which the variants had generated. Solutions exceeding a misorientation of 8° were discarded from the original dataset as a compromise to reconstruct the parent  $\beta$  phase with certainty and be able to generate an orientation map from a representative number of data points.

### 3. Results and Discussion

Ti-6Al-4V is an allotropic alloy organised in a  $\beta$  phase above the  $\beta$  transus temperature of the alloy (typically above 950°C) and in a  $\alpha+\beta$  phase below this critical temperature. Nevertheless the amount of retained  $\beta$  phase at room temperature is dictated by the cooling rate experienced by the alloy and because during SLM each layer cools down very rapidly (orders of thousands degrees per second) the components can be expected to be completely  $\alpha'$  phase [13,14]. The optical microscopy analysis reveals in fact that the microstructure of the builds is composed of fine acicular  $\alpha'$  grains throughout the sample (Figure 3A) as it will be demonstrated hereafter by TEM investigations. In this study, the  $\alpha'$  grains do not vary with distance from the building platform or across the scanning plane. This is due to the fact that the building platform, kept at a low temperature, did not contribute to the evolution of the as deposited phase during the building process. It has been reported in fact for electron beam melting or laser metal deposition the builds sit at 500 to 800°C for several hours and as result of this the  $\alpha$  grain size varies on different sample locations depending on the sample size and geometry [15,16]. This suggests the importance of the build chamber temperature in the microstructure evolution and implies that the meander scanning strategy alone cannot bias either a  $\alpha'$  to  $\alpha$  decomposition or  $\alpha'$  grain growth.

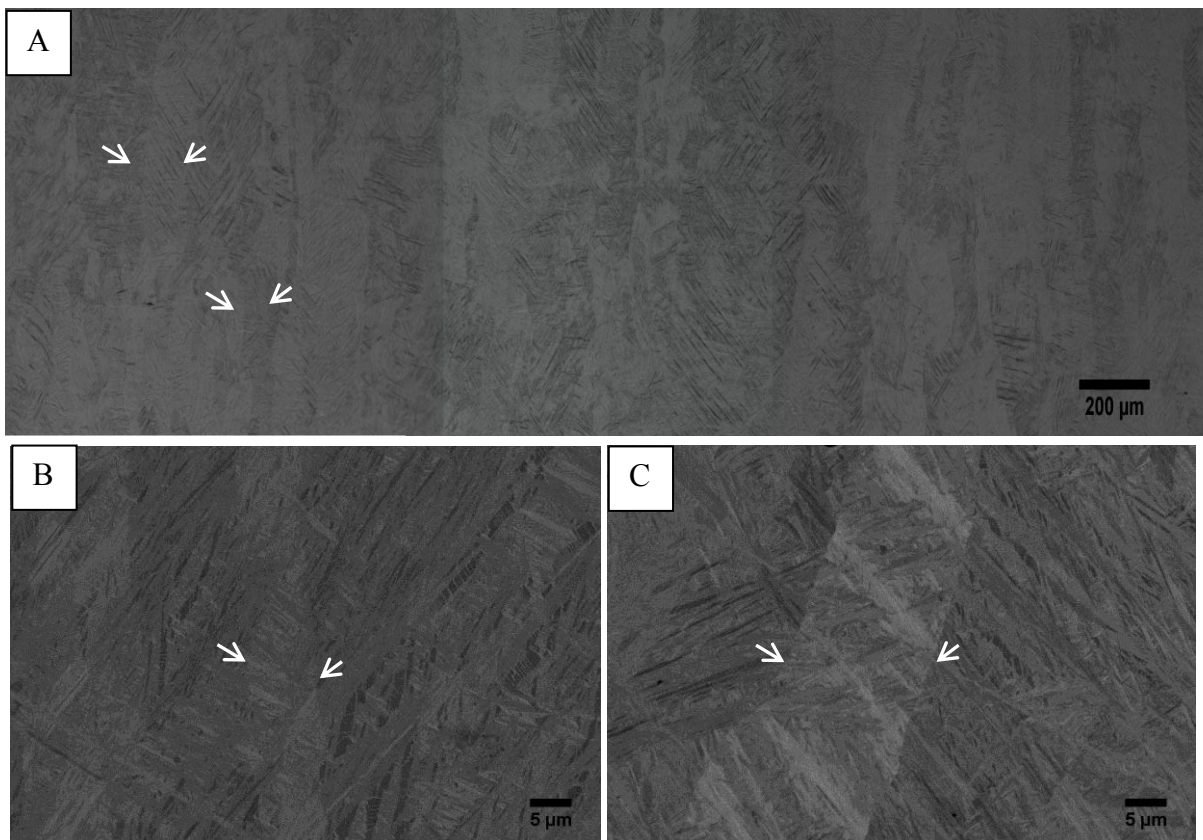


**Figure 3:** A) Optical micrograph montage showing the microstructure of a section parallel to the building direction of as-fabricated SLM Ti-6Al-4V (prior  $\beta$  columnar grain boundaries indicated by the arrows); B) and C) Backscattered electron images from the same section showing the morphology and the arrangement of the  $\alpha'$  laths within the prior  $\beta$  columnar grains

The  $\alpha'$  martensitic phase is organized within prior  $\beta$  grain boundaries (Figure 3A, B and C) with different inclinations of  $\pm 45^\circ$  and  $90^\circ$  to the building direction as reported elsewhere [3,6]. The  $\alpha'$  grains do not precipitate along the  $\beta$  grain boundaries (Figure 3C) and this suggests that the  $\alpha'$  originates simultaneously from different points within the parent  $\beta$  grain as typical of martensitic transformations [17]. This can be explained considering the large cooling rate typical of SLM. The prior  $\beta$  grain boundaries are continuous with an average width of  $62 \pm 12 \mu\text{m}$ . It has been reported that the width of the prior  $\beta$  grains is related to the hatch spacing (unitary ratio) although in this is not the case for the present study where the hatch spacing was kept at  $100 \mu\text{m}$  [4]. As mentioned, the presence of the prior  $\beta$  columnar grain boundaries is explained by the fact that Ti-6Al-4V solidifies in the  $\beta$  phase field and heat is mainly conducted away vertically. As the scanning direction is rotated by  $67^\circ$  at each layer the prior  $\beta$  columnar grain boundaries are vertical and appear not to be skewed towards any direction in contrast to that reported for SLM Ti-6Al-4V when the scanning direction was rotated by  $90^\circ$  at each layer [4]. The martensitic nature of the  $\alpha'$  grains was confirmed studying the crystallographic structure and the chemistry of the laths under TEM. The  $\alpha'$  grains appear as relatively long and narrow laths characterized by high dislocation density stacking faults and twin structures (Figure 4A and 4B).

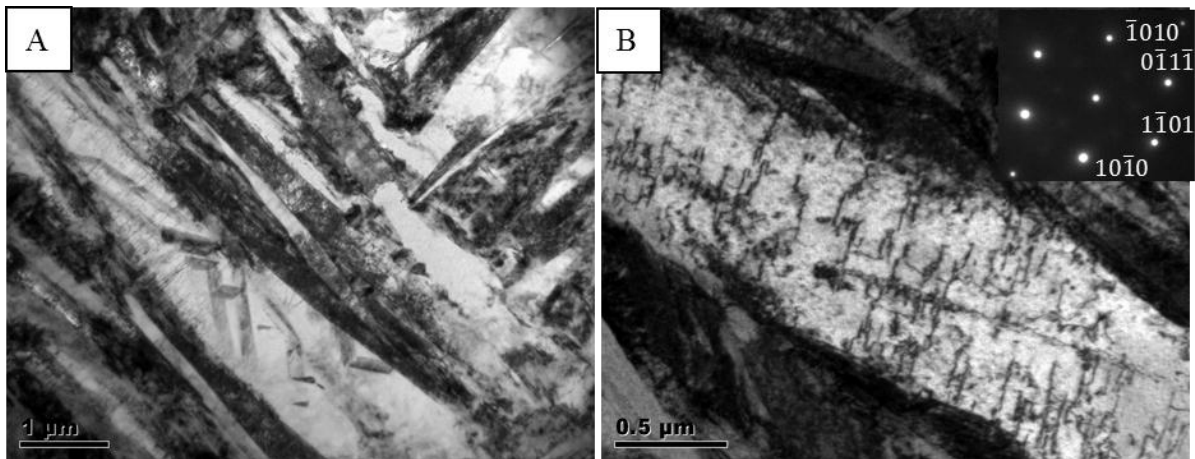


**Figure 4:** A) Bright field TEM showing the morphology of several  $\alpha'$  grains, B) Typical substructure of the  $\alpha'$  grains; inset showing a selected area diffraction pattern relative to the  $\alpha'$  grain shown in Figure 4B. The orientation of the beam was  $\langle 1\bar{2}13 \rangle$

In recent years crystallographic texture information has shown to be extremely useful and complementary to the standard microstructural studies because micro-texture plays a crucial role in the mechanical performance of several  $\alpha+\beta$  Ti alloys [18-20]. For this reason an EBSD analysis on a frontal section of as deposited materials was carried out. The corresponding inverse pole figure orientation map (RD-TD plane) is shown in Figure 5A. This  $\alpha'$  texture study reveals that there isn't a prevailing strong orientation texture (Figure 5A and C). A relatively high number of variants within each single prior  $\beta$  grain can be noticed (Figure 5A). Similar textures have been reported for Ti-6Al-4V processed by other AM technologies [15] although the micro-texture of as fabricated SLM doesn't show any colony



formation of  $\alpha$  laths sharing the same crystallographic orientation. However, few crystal orientations tend to repeat within the same prior  $\beta$  grain (e.g. Figure 5A prior  $\beta$  grain 1 and 2), as indicated by the repetition of the same colour of the  $\alpha'$  grains, suggesting that texture inheritance and variant selection have taken place. In other words when the room temperature  $\alpha'$  phase is heated in the  $\beta$  phase field and cooled down to room temperature again the same variants are formed [11,12].

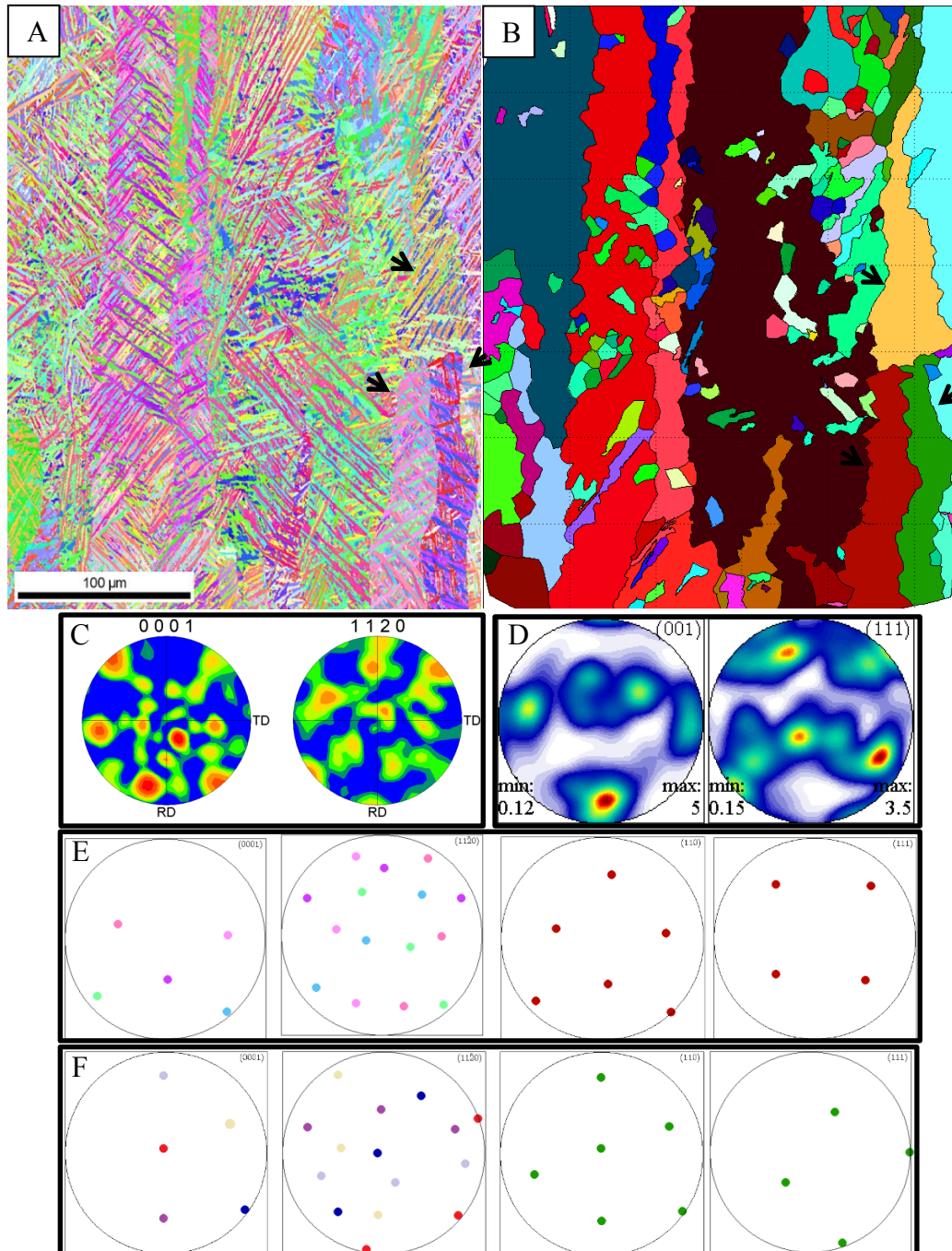


**Figure 5:** A) Orientation map of the frontal section of as-built SLM Ti-6Al-4V  $\alpha'$  phase and B) the reconstructed prior  $\beta$  grains. C) Contour and pole figures corresponding to the whole section in analysis of the  $\alpha'$  phase and D) the reconstructed  $\beta$  phase. E) and F) Orientation relationship of the  $\alpha'$  laths belonging to two indicated prior  $\beta$  grains

In order to clarify this aspect, a detailed analysis of the variants within several prior  $\beta$  grains and their relationship with their parent  $\beta$  phase were analysed. As a typical example, the orientation of the  $\alpha'$  laths belonging to the two labelled grains in Figure 5A and their orientation relationship with the parent phase is reported in Figure 5E and 5F. Typically 5 to 6 variants are formed inside every parent  $\beta$  grain and, as expected, the  $\beta \rightarrow \alpha'$  transformation follows the Burgers orientation relationship; the  $(0001)_{\alpha'}$  poles are parallel to one of the  $(110)_{\beta}$  poles of the reconstructed parent phase and at least one of the  $\langle 11\bar{2}0 \rangle_{\alpha'}$  directions is parallel to one of the  $\langle 111 \rangle_{\beta}$  (Figure 5E and 5F). It was noticed that most of the analysed grains had the  $(0001)_{\alpha'}$  poles  $60^\circ$  misoriented around the  $\langle 01\bar{1}0 \rangle_{\alpha'}$  axes of rotation. Only occasionally different  $\alpha'$  grains belonging to the same parent  $\beta$  grain shared a  $(0001)_{\alpha'}$  reflection. The  $(11\bar{2}0)_{\alpha'}$  pole figures corresponding to the  $\alpha'$  grains with distinct  $(0001)_{\alpha'}$  reflections did not show any specific geometric pattern contrary to that observed for Ti-6Al-4V fabricated by other AM technologies [21]. The reported triangular or rhombic patterns of the  $(11\bar{2}0)_{\alpha'}$  pole figures are in fact a result of  $\alpha'$  grains with different two or three different basal poles and at least one common  $(11\bar{2}0)_{\alpha'}$  pole [22,23]. This orientation relationship never occurred in the present case study. The few  $\alpha'$  grains sharing the  $(0001)_{\alpha'}$  pole had, however, the three  $(11\bar{2}0)_{\alpha'}$  reflections misoriented by  $10.53^\circ$  around the  $\langle 0001 \rangle_{\alpha'}$  axes (Figure 6). The only occasions when this happened was in correspondence to two  $\alpha'$  grains appearing in two different shades of the same colour (e.g. Figure 5A, grain3). This particular orientation relationship can be explained considering the 6-fold symmetry of the HCP lattice and by the fact that during the  $\beta \rightarrow \alpha'$  transformation the  $\langle 11\bar{2}0 \rangle_{\alpha'}$  direction remains parallel to the two possible  $\langle 111 \rangle_{\beta}$  close packed directions that lie on the  $\{110\}_{\beta}$  plane [23].

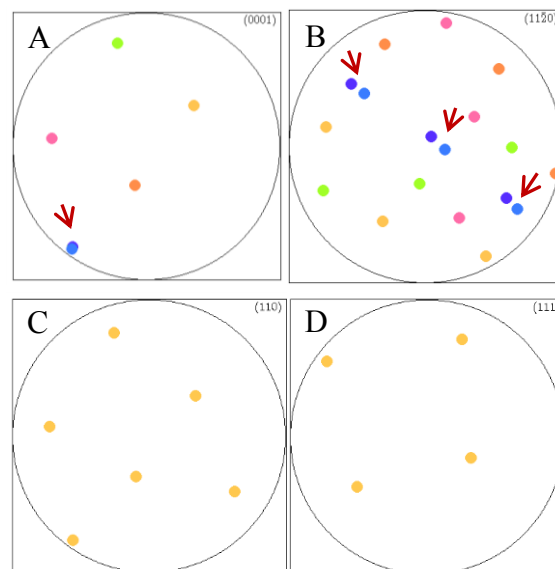


**Figure 6:** A) and B)  $(0001)$  and  $(11\bar{2}0)$  pole figures of the  $\alpha'$  laths of grain indicated in Figure 5B; the red arrows indicate the two variants that share a common  $(0001)$  pole and have the  $(11\bar{2}0)$  reflections misoriented by  $10.53^\circ$ ; C) and D)  $(110)$  and  $(111)$  pole figures of the reconstructed prior  $\beta$  grain 3



In order to understand whether all the 12  $\alpha'$  variants were developed with equal probability, statistics regarding the variant frequency was determined for the dataset under analysis. The 12  $\alpha'$  variants were not developed equally during cooling as shown in Figure 7. Instead, certain variants were formed more frequently than the others: the  $D^{-1}C_{4x+}$ ,  $D^{-1}C_{2z}$  solutions were favoured having a frequency of 17% followed by solutions  $D^{-1}C_{32-}$ ,  $D^{-1}E$  and  $D^{-1}C_{4z-}$  (13%). Solutions  $D^{-1}C_{31+}$  and  $D^{-1}C_{4z-}$  never occurred. The reason behind this variant selection is subject of on-going work. The fact the only a subset of the 12 different possibilities for the  $\beta \rightarrow \alpha'$  transformation take place however is interesting because demonstrates that if the prior  $\beta$  grains morphology and texture is controlled during processing the final micro texture of the components can be tailored as well.

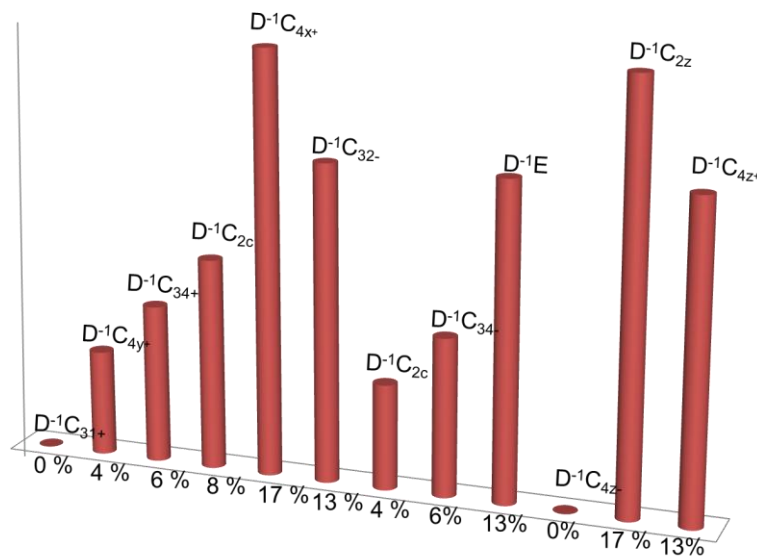


**Figure 7:** Variant frequency distribution originated from several grains studied in Figure 5

For this reason the texture of the prior  $\beta$  phase was calculated. Figure 5C represent the orientation map of the reconstructed  $\beta$  phase. The black lines in the orientation map of Figure 5C represent high angle grain boundaries ( $>10^\circ$ ). As expected the grain boundaries of the reconstructed map match with the prior  $\beta$  columnar grain boundaries of Figure 5A revealing once again that columnar epitaxial growth of the  $\beta$  phase. The  $\beta$  grains texture reminds of the standard  $\langle 100 \rangle$  solidification texture of the BCC materials, although it is slightly deviated towards the  $\langle 111 \rangle$  texture. This result is analogous to what reported for electron beam melted Ti-6Al-4V where a strong predominance of the  $\langle 100 \rangle$  was found [15]. Varying the scan direction at each layer seems then not to impose any particular preferred texture other than the  $\langle 100 \rangle$  solidification texture. The correlation between the laser beam motion and the crystallographic texture of the  $\beta$  phase will be studied further in order to understand whether the scan strategy could be used to grow  $\beta$  grains with a desired direction, size and orientation.

#### 4. Conclusion

The objective of this study was to understand the evolution of the microstructure and the texture of Ti-6Al-4V fabricated using a set of process parameters that enabled the production of near fully dense parts. This study has shown that the as-fabricated components consist entirely of  $\alpha'$  martensitic phase as confirmed by TEM diffraction pattern analysis and TEM-EDX. It was found that the  $\alpha'$  grains precipitate and replace entirely the prior parent  $\beta$  grains leaving behind the grain boundaries only. It was demonstrated that the width of the prior  $\beta$  columnar grains is correlated to the hatch spacing and that rotating the scan direction at each layer SLM Ti-6Al-4V solidifies vertically and almost parallel to the building direction. Although the  $\alpha'$  texture of the as-fabricated components appears random due the high number of formed variants, texture inheritance and variant selection takes place. It was found that the  $\beta \rightarrow \alpha'$  transformation is governed by the Burgers orientation relationship: most of the  $\alpha'$  laths belonging to the same parent  $\beta$  grain have the  $(0001)_{\alpha'}$  reflection  $60^\circ$  misoriented around the  $\langle 01\bar{1}0 \rangle_{\alpha'}$  axes of rotation whereas the  $(11\bar{2}0)_{\alpha'}$  reflections don't seem to follow a precise pattern. Interestingly some of the 12 possible variants occur more frequently than others in the present dataset: this is an encouraging result for SLM of  $\alpha/\beta$  Ti alloys because it demonstrates that if the  $\beta$  phase solidification texture is controlled also the  $\alpha'$  phase texture can be tailored. Varying the scan strategy at each layer doesn't alter significantly the standard solidification  $\langle 100 \rangle$  texture of the parent  $\beta$  phase. Further studies on the correlation of the scan strategy and the solidification texture are on-going. One of the key challenges for SLM is the possibility to tailor the microstructure during the building process: the first step was, however, to comprehend the relationship among the microstructural features of SLM Ti-6Al-4V. Microtexture contains all the information that explains the effect of the adopted process parameters and should be considered a tool of investigation for the production of tailored SLM microstructures.

## 5. References

1. Reeves P. Additive Manufacturing—A supply chain wide response to economic uncertainty and environmental sustainability. Econolyst Limited, The Silversmiths, Crown Yard, Wirksworth, Derbyshire, DE4 4ET, UK .
2. Gebhardt A, Schmidt F, Hötter J, Sokalla W, Sokalla P. Additive Manufacturing by selective laser melting the realizer desktop machine and its application for the dental industry. *Physics Procedia* 2010;5, Part B:543-549.
3. Sercombe T, Jones N, Day R, Kop A. Heat treatment of Ti-6Al-7Nb components produced by selective laser melting. *Rapid Prototyping Journal* 2008;14:300-304.
4. Thijs L, Verhaeghe F, Craeghs T, Humbeeck JV, Kruth JP. A study of the microstructural evolution during selective laser melting of Ti-6Al-4V. *Acta Materialia* 2010;58:3303-3312.
5. Gu D, Hagedorn Y, Meiners W, Meng G, Batista RJS, Wissenbach K, Poprawe R. Densification behavior, microstructure evolution, and wear performance of selective laser melting processed commercially pure titanium. *Acta Materialia* 2012;60:3849-3860.
6. Facchini L, Magalini E, Robotti P, Molinari A, Hoeges S, Wissenbach K. Ductility of a Ti-6 Al-4 V alloy produced by selective laser melting of prealloyed powders. *Rapid Prototyping Journal* 2010;16:450-459.
7. Chlebus E, Kuznicka B, Kurzynowski T, Dybala B. Microstructure and mechanical behaviour of Ti-6Al-7Nb alloy produced by selective laser melting. *Mater Charact* 2011.
8. Song B, Dong S, Zhang B, Liao H, Coddet C. Effects of processing parameters on microstructure and mechanical property of selective laser melted Ti6Al4V. *Mater Des* 2012;35:120-125.
9. Zhang L, Klemm D, Eckert J, Hao Y, Sercombe T. Manufacture by selective laser melting and mechanical behavior of a biomedical Ti-24Zr-4Nb-7.9 Sn alloy. *Scr Mater* 2011.
10. Thomas Vilaro, V. Kottman-Rexerodt, Marc Thomas, Christophe Colin, P. Bertrand, L. Thivillon, S. Abed, V. Ji, P. Aubry, Patrice Peyre, T. Malot. Direct Fabrication of a Ti-47Al-2Cr-2Nb Alloy by Selective Laser Melting and Direct Metal Deposition Processes. *Advanced Materials Research* 2010;89-91:586-591.
11. Lonardelli I, Gey N, Wenk H-, Humbert M, Vogel SC, Lutterotti L. In situ observation of texture evolution during  $\alpha \rightarrow \beta$  and  $\beta \rightarrow \alpha$  phase transformations in titanium alloys investigated by neutron diffraction. *Acta Materialia* 2007;55:5718-5727.
12. Daymond MR, Holt RA, Cai S, Mosbrucker P, Vogel SC. Texture inheritance and variant selection through an hcp–bcc–hcp phase transformation. *Acta Materialia* 2010;58:4053-4066.

13. Roberts IA, Wang CJ, Esterlein R, Stanford M, Mynors DJ. A three-dimensional finite element analysis of the temperature field during laser melting of metal powders in additive layer manufacturing. *International Journal of Machine Tools and Manufacture* 2009;49:916-923.
14. T V, C C, JD B. As-Fabricated and Heat-Treated Microstructures of the Ti-6Al-4V Alloy Processed by Selective Laser Melting. *METALLURGICAL AND MATERIALS TRANSACTIONS A* 2011;42:3190-3199.
15. Al-Bermani S, Blackmore M, Zhang W, Todd I. The Origin of Microstructural Diversity, Texture, and Mechanical Properties in Electron Beam Melted Ti-6Al-4V. *Metallurgical and Materials Transactions A* 2010;41:3422-3434.
16. Facchini L, Magalini E, Robotti P, Molinari A. Microstructure and mechanical properties of Ti-6Al-4V produced by electron beam melting of pre-alloyed powders. *Rapid Prototyping Journal* 2009;15:171-178.
17. Ahmed T, Rack H. Phase transformations during cooling in [alpha] [beta] titanium alloys. *Materials Science and Engineering A* 1998;243:206-211.
18. Glavicic M, Kobryn P, Bieler T, Semiatin S. An automated method to determine the orientation of the high-temperature beta phase from measured EBSD data for the low-temperature alpha-phase in Ti-6Al-4V. *Materials Science and Engineering A* 2003;351:258-264.
19. Glavicic M, Kobryn P, Semiatin S. Validation of an automated EBSD method to deduce the [beta]-phase texture in Ti-6Al-4V with a colony-[alpha] microstructure. *Materials Science and Engineering A* 2004;385:372-376.
20. Kobryn P, Semiatin S. Microstructure and texture evolution during solidification processing of Ti-6Al-4V. *J Mater Process Technol* 2003;135:330-339.
21. Baufeld B, Van der Biest O, Dillien S. Texture and crystal orientation in Ti-6Al-4V builds fabricated by shaped metal deposition. *Metallurgical and Materials Transactions A* 2010:1-11.
22. Bhattacharyya D, Viswanathan GB, Fraser HL. Crystallographic and morphological relationships between  $\beta$  phase and the Widmanstätten and allotriomorphic  $\alpha$  phase at special  $\beta$  grain boundaries in an  $\alpha/\beta$  titanium alloy. *Acta Materialia* 2007;55:6765-6778.
23. Bhattacharyya D, Viswanathan G, Denkenberger R, Furrer D, Fraser HL. The role of crystallographic and geometrical relationships between [alpha] and [beta] phases in an [alpha]/[beta] titanium alloy. *Acta materialia* 2003;51:4679-4691.